The Impact of Spatial Self-Shielding on Pin-Wise Reaction Rates

William Boyd, Benoit Forget, Kord Smith

Massachusetts Institute of Technology, Department of Nuclear Science and Engineering, 77 Massachusetts Avenue, Building 24, Cambridge, MA 02139, United States

Abstract

Keywords: Multi-group cross-sections, spatial homogenization, spatial self-shielding

1. Introduction

The nuclear reactor physics community has long strived for deterministic neutron transport-based tools for whole-core reactor analysis. A key challenge for whole-core multi-group transport methods is accurate reactor agnostic multi-group cross section (MGXS) generation. The MGXS generation process applies a series of approximations to produce spatially homogenized and energy condensed MGXS in each spatial zone and energy group. ... However, the practical impact of ... is less understood. This paper investigates the ... and quantifies its significance for heterogeneous PWR problems.

This work employs Monte Carlo (MC) neutron transport simulations to generate MGXS. Monte Carlo methods have increasingly been used to generate few group constants for coarse mesh diffusion, most notably by the Serpent MC code (Leppänen, 2013), and to a much lesser extent, for high-fidelity neutron transport methods (Redmond, 1997; Nelson, 2014; Cai, 2014; Boyd, 2016). The advantage of a MC-based approach is that all of the relevant physics are directly embedded into MGXS by weighting the continuous energy cross sections with a statistical proxy to the "true" neutron flux.

This paper seeks to identify the bias between continuous energy and multi-group transport methods for MGXS libraries which account for spatial self-shielding effects[1] to varying degrees. In particular, this paper quantifies the difference in the approximation error between simulations in which the same MGXS are used in each unique fuel pin (*e.g.*, each fuel enrichment) and those in which unique MGXS are used in each and every pin. The former case does little if anything to model spatial self-shielding effects, whereas the latter case "fully" resolves these effects, albeit at the expense of very large MGXS libraries.

The content in this paper is organized as follows. Two different schemes for spatial homogenization of pin-wise MGXS are introduced in Sec. 2. The need for a new, more flexible and specialized approach to spatial homogenization which appropriately captures spatial self-shielding effects with minimal computational expense is discussed in Sec. 5.

Email addresses: wboyd@mit.edu (William Boyd), bforget@mit.edu (Benoit Forget), kord@mit.edu (Kord Smith)

[1] The effects of neighboring pins, burnable poisons, reflectors and the core baffle are each of interest in the context of spatial self-shielding.

2. Methodology

This work required the development of a "simulation triad" encompassing three primary simulation tools. First, the OpenMC Monte Carlo code (Romano and Forget, 2013) was utilized to generate multi-group cross sections. Second, the MGXS were used by the OpenMOC code (Boyd et al., 2014) for deterministic multi-group transport calculations. Third, the OpenCG library (Boyd et al., 2015) enabled the processing and transfer of tally data on combinatorial geometry (CG) meshes between OpenMC and OpenMOC. Each of the OpenMC, OpenMOC, and OpenCG codes is highlighted in Sec. 2.1, Sec. 2.2 and **??**.

-outline sections for spatial homogenization?? probably needs further motivating

2.1. Continuous Energy Calculations with OpenMC

The OpenMC continuous energy Monte Carlo (MC) code (Romano and Forget, 2013) was employed to generate multi-group cross sections, and reference eigenvalues and pin-wise fission and capture reaction rates. The `openmc.mgxs` Python module was used to tally multi-group cross sections in CASMO's seventy energy group structure (Rhodes et al., 2006) from a single eigenvalue calculation. The multi-group cross sections were calculated with OpenMC's distributed cell tally algorithm (Lax et al., 2014), which permits spatial tally zones across repeated cell instances. In particular, unique MGXS were computed for each fuel pin cell with distributed cell tallies in the repeating lattice benchmarks described in Sec. 3.

The OpenMC simulations used the "iso-in-lab" feature to enforce isotropic in lab scattering. The "iso-in-lab" feature samples the outgoing neutron energy from the scattering laws prescribed by the continuous energy cross section library, but the outgoing neutron direction of motion is sampled from an isotropic in lab distribution. Although isotropic in lab scattering is a poor approximation for LWRs, it eliminated scattering source anisotropy as one possible cause of approximation error between OpenMC and OpenMOC. This simplification made it possible to isolate the approximation error resulting from the spatial self-shielding model used to generate MGXS, which is the focal point of this paper.

2.2. Multi-Group Calculations with OpenMOC

The OpenMOC code (Boyd et al., 2014) was employed to use the MGXS generated by OpenMC for deterministic multi-

group calculations. The OpenMOC code is a 2D method of characteristics code designed for fixed source and eigenvalue neutron transport calculations. OpenMOC approximates the scattering source as isotropic in the lab coordinate system, and discretizes the geometry into flat source regions (FSRs) which approximate the neutron source as constant across each spatial zone. The OpenMOC eigenvalue and energy-integrated, pin-wise reaction rates were compared with the reference solution computed by OpenMC.

Each OpenMOC simulation used a characteristic track laydown with 128 azimuthal angles and 0.05 cm spacing. All eigenvalue calculations were converged to 10^{-5} on the root mean square of the energy-integrated fission source in each FSR. The Coarse Mesh Finite Difference (CMFD) acceleration scheme was employed on a pin-wise spatial mesh to reduce the number of iterations required to converge the fine-mesh transport calculations. The 70-group MGXS used for MOC were collapsed to a 14-group structure for CMFD to significantly improve the speed of the CMFD eigenvalue calculations.

2.3. Pin-wise Spatial Homogenization Schemes

-single level Monte Carlo calculation -focus less on introducing these as "schemes" per se -rather two spatial self-shielding models to quantify approx. error

This paper employs two different spatial homogenization schemes to model spatial self-shielding effects in MGXS. Although all spatial zones may experience spatial self-shielding, this chapter only models the impact of spatial self-shielding on MGXS in fissile regions. The null and degenerate spatial homogenization schemes are introduced in Sec. 2.3.1 and Sec. 2.3.2, respectively. These schemes model spatial self-shielding for each fuel pin with increasing granularity and complexity. A fuel assembly and 2×2 colorset with reflector model are color-coded by material and illustrated in Fig. 1 for each homogenization scheme.

The `openmc.mgxs` module was used to compute 70-group MGXS with OpenMC for both the assembly and colorset benchmarks. The tallied MGXS data was condensed to coarse 2-group and 8-group structures with downstream data processing as necessary. The OpenMC simulations were performed with 1000 batches with 10^6 particle histories per batch for each benchmark. Stationarity of the fission source was obtained with 100 inactive batches for each benchmark. OpenMC's "iso-in-lab" feature was employed to enable consistent comparisons between OpenMC's reference results and OpenMOC's calculations with an isotropic in lab scattering source.

2.3.1. Null Homogenization

The *null* spatial homogenization scheme uses a single Monte Carlo calculation of the complete heterogeneous geometry to generate MGXS for each material. In this way, the null scheme fully abandons the multi-level approach used by most traditional approaches to generate MGXS. The spatially self-shielded flux is used to collapse the cross sections in each material with a unique isotopic composition. The null scheme does not account for spatial self-shielding effects experienced by different fuel pins filled by the same type of fuel, and instead averages these effects across the entire geometry. A single MGXS is employed in each instance of a material zone, such as a fuel pin replicated many times throughout a benchmark geometry.

2.3.2. Degenerate Homogenization

Unlike the null scheme, the *degenerate* scheme accounts for the different spatial self-shielding effects experienced by each instance of each fuel pin throughout a heterogeneous geometry. Like the null scheme, a single MC calculation of the complete heterogeneous geometry is used to generate MGXS for all materials. Unlike the null scheme, the MGXS are tallied separately for each instance of fissile material zones. For example, if a heterogeneous benchmark includes N fuel pins, then N collections of MGXS are separately tabulated for each fuel pin instance. The degenerate scheme tallies different MGXS even if the isotopic compositions in the fuel pin instances are identical (*e.g.*, fresh fuel at the beginning of life) since each instance may experience different spatial self-shielding effects and hence have different MGXS.

The degenerate scheme generates MGXS for each fuel pin instance using OpenMC's distributed cell tallies (Lax et al., 2014). The OpenCG region differentiation algorithm (Boyd et al., 2015) is used to build a new OpenMOC geometry with unique cells and materials for each fuel pin. The MGXS are appropriately selected from OpenMC's distributed cell tallies to populate the MGXS in the OpenMOC materials. Multi-group transport calculations with MGXS generated using null and degenerate schemes may be compared to quantify the impact of modeling spatial self-shielding effects in MGXS for fissile zones in heterogeneous geometries.

3. Test Cases and Reference Results

This paper models two test cases derived from the Benchmark for Evaluation And Validation of Reactor Simulations (BEAVRS) PWR model (Horelik et al., 2013). Each test case includes heterogeneous features – and corresponding spatial self-shielding effects – in order to understand their implications for accurate pin-wise MGXS generation. Although BEAVRS is an axially heterogeneous 3D core model, both benchmarks were fabricated in 2D due to the geometric constraints in OpenMOC. The impact of fuel enrichment, CRGTs, BPs, inter-assembly currents and water reflectors is considered. The geometric and material specifications for the two test cases are summarized in Sec. 3.1. The reference results computed with OpenMC are discussed in Sec. 3.2.

3.1. Benchmark Configurations

The two test cases were comprised of materials from the BEAVRS model, including 1.6% and 3.1% enriched UO_2 fuel, borated water[2], zircaloy, helium, air, borosilicate glass and

[2]The water consisted of 975 parts per million (ppm) boron.

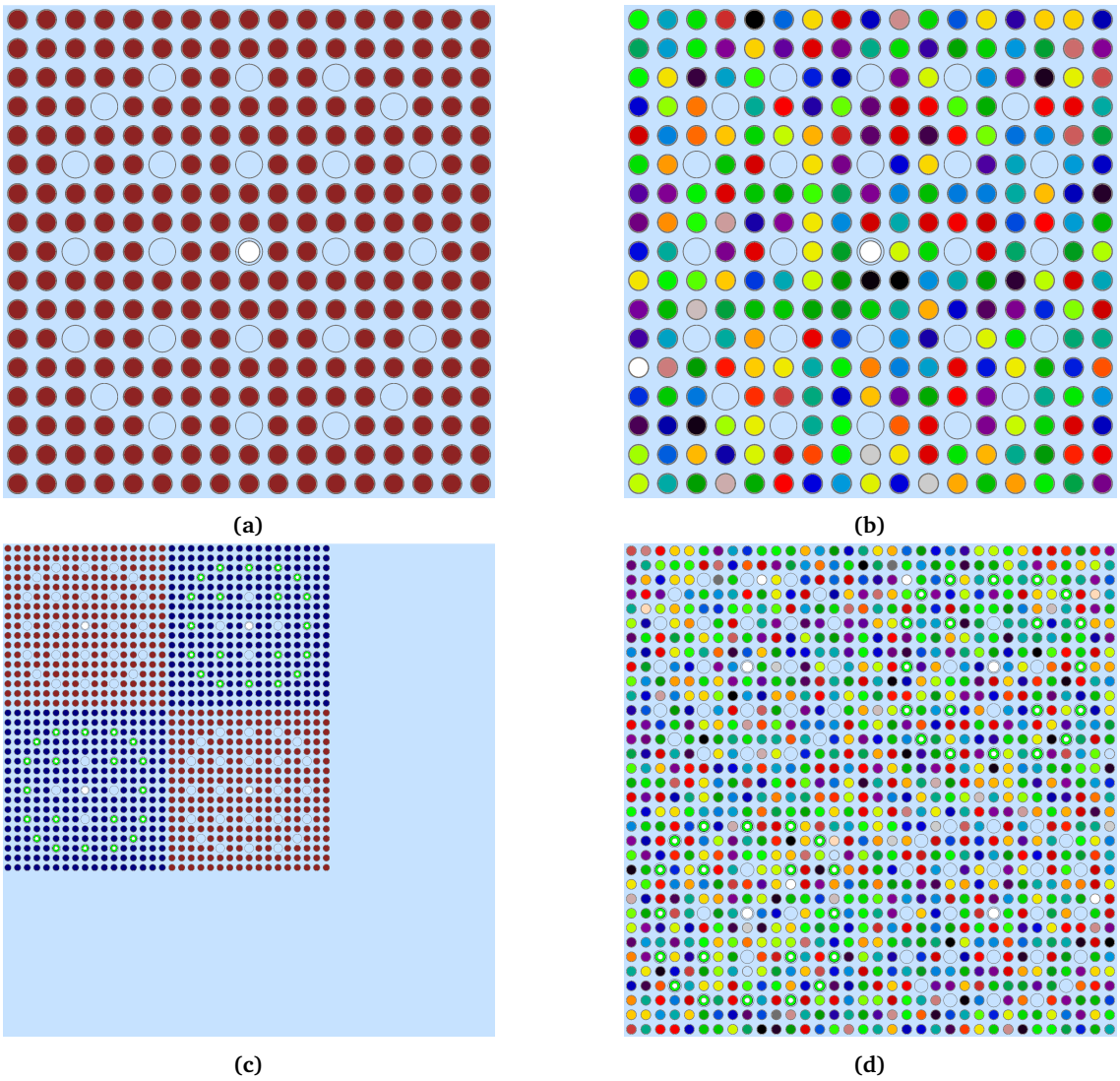

Figure 1. OpenMOC materials for the (a)-(b) assembly and (c)-(d) 2×2 colorset models with null and degenerate homogenization, respectively.

stainless steel. The densities and isotopic compositions for each material are detailed in the BEAVRS specifications (Horelik et al., 2013). Each material was modeled with cross sections from the ENDF/B-VII.1 continuous energy cross section library (X-5 Monte Carlo Team, 2003) evaluated at 600K for hot zero power conditions.

The first benchmark was a single fuel assembly with an array of 264 fuel pins of 1.6% enriched UO_2 fuel with zircaloy cladding and a helium gap as illustrated in Fig. 2a. The assembly included 24 CRGTs of borated water surrounded by zircaloy cladding, and a central instrument tube filled with air surrounded by two zircaloy tubes separated by borated water. The intra-pin egg-crate grid spacer and grid sleeve separating each assembly in the BEAVRS model were not included in the assembly benchmark. The assembly was modeled with reflective boundary conditions.

The second benchmark was constructed as a 2×2 colorset of two fuel assemblies extracted from the BEAVRS model. The top-left and bottom-right fuel assemblies in the colorset were of the same enrichment and configuration as the first benchmark configuration. The top-right and bottom-left fuel assemblies included 264 fuel pins of 3.1% enriched UO_2 fuel, 20 CRGTs and a central instrument tube. In addition, the two 3.1% enriched assemblies included four BPs consisting of eight layers of air, steel, borosilicate glass and zircaloy. The colorset was surrounded by a water reflector on the bottom and right that was of the same width as a fuel assembly. The reflected colorset included reflective boundaries on the top and left (adjacent to the fuel assemblies) with vacuum boundaries on the bottom and right (adjacent to the reflector).

Flat source region spatial discretization meshes were applied to both benchmarks for the OpenMOC simulations as shown in Fig. 3. Eight equal angle subdivisions were used in all material zones. The UO_2 fuel was subdivided into five equal volume radial rings, while ten radial rings were employed in the water-filled CRGTs and instrument tubes. The borosilicate glass and borated water material zones filling the BPs were each discretized into five equal volume radial rings.

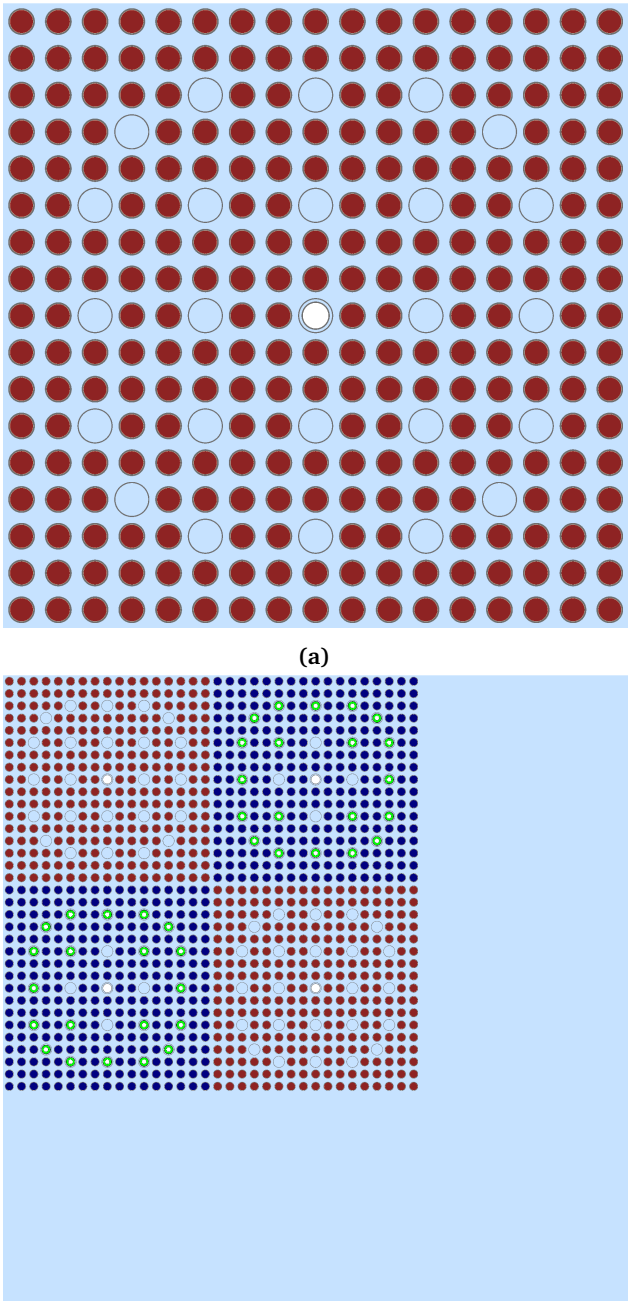

(a)

(b)

Figure 2. The (a) fuel assembly and (b) colorset with reflector benchmarks.

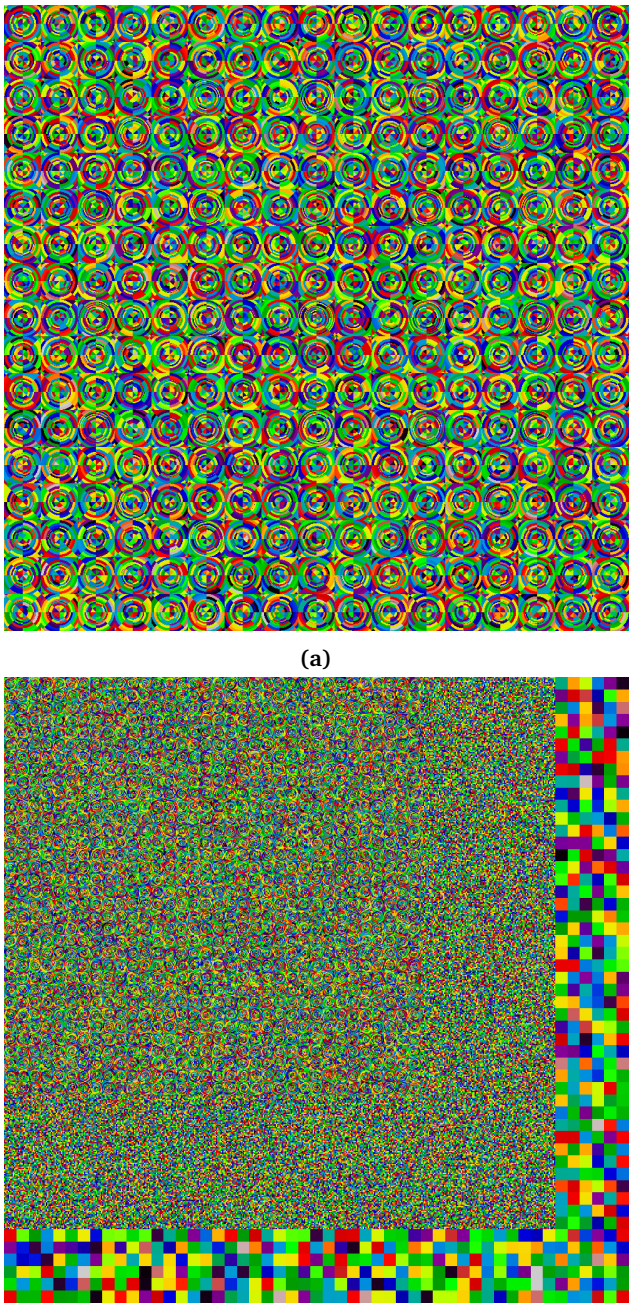

(a)

(b)

Figure 3. FSRs for the (a) fuel assembly and (b) colorset with reflector.

Finally, five equally spaced rings were used in the moderator zones surrounding each pin. The 13.85824 cm of water reflector nearest the fuel assemblies in the colorset benchmark was discretized in a 0.125984 cm × 0.125984 cm rectilinear mesh, equivalent to a 10×10 mesh in each pin. The of 7.55904 cm of reflector furthest from the fuel assemblies was discretized in a 1.25984 cm × 1.25984 cm pin-wise mesh.

3.2. Verification Metrics

A series of OpenMC simulations were used to calculate reference eigenvalues, pin-wise fission rates, and pin-wise U-238 capture rates for both benchmarks. The reference solutions were computed with 100 inactive and 900 active batches of 10^7 particle histories per batch. The reference eigenvalues are listed in Tab. 1. The OpenMC "combined" eigenvalue estimator is reported along with the associated 1-sigma uncertainty of one pcm for both test cases.

The reference energy-integrated fission and U-238 capture rate spatial distributions were computed using rectilinear, pin-wise tally meshes in OpenMC and are shown in Fig. 4. The reaction rates were volume-integrated across each fuel pin. The fission rates include fission from only U-235 and U-238 for

Table 1. Reference OpenMC eigenvalues for each test case.

Assembly	Colorset
0.99326 ± 0.00001	0.94574 ± 0.00001

the fresh PWR UO_2 fuel. The reaction rates were normalized to the mean of all non-zero reaction rates in each benchmark. The reaction rates in the instrument tubes, CRGTs and BPs are all zero and are illustrated in white. The 1-sigma uncertainties are less than 0.08% in each pin for each benchmark.

As illustrated in the figures, the reaction rate rate distributions are strongly dependent on the spatially heterogeneous features in each benchmark. For example, the CRGTs provide additional moderation and increase the fision and U-238 capture rates in nearby fuel pins. The inclusion of BPs reduces the neutron population and therefore the reaction rates for the surrounding fuel pins. The presence of a reflector with a mixture of vacuum and reflective BCs induces a tilt in the reaction rates across the assemblies in the colorset.

Although spatial heterogeneities generally have similar effects on both fission and U-238 capture rates, there are a few important differences to note. The U-238 capture rates in the assemblies are more sensitive than the fission rates to the spatial self-shielding induced by moderation in CRGTs. In addition, the capture rates in the colorset are more smoothly varying at the inter-assembly and assembly-reflector interfacea than the fission rates.

4. Results

4.1. Eigenvalues

In the results that follow, the bias $\Delta\rho$ compares the eigenvalue k_{eff}^{MOC} computed by OpenMOC to that of the reference eigenvalue k_{eff}^{MC} computed by OpenMC in units of pcm:

$$\Delta\rho = \left(k_{eff}^{MOC} - k_{eff}^{MC}\right) \times 10^5 \quad (1)$$

Table 2. OpenMOC eigenvalue bias $\Delta\rho$.

Benchmark	Null	Degenerate
Assembly	-161	-161
Colorset	-142	-132

4.2. Fission Rates

-add figures of spatial distribution of errors -can I reproduce these plots? Do I have the batchwise.h5 results stored on my external hard drive??? If so, I should customize them for only 70 groups

4.3. Capture Rates

-add figures of spatial distribution of errors

Table 3. OpenMOC fission rate percent relative errors.

Benchmark	Metric	Null	Degenerate
Assembly	Max	0.380	0.315
	Mean	0.074	0.079
Colorset	Max	0.764	0.602
	Mean	0.178	0.138

Table 4. OpenMOC U-238 capture rate percent relative errors.

Benchmark	Metric	Null	Degenerate
Assembly	Max	-1.101	0.386
	Mean	0.479	0.086
Colorset	Max	-1.969	-0.783
	Mean	0.478	0.165

5. Conclusions

Acknowledgments

This work was supported by the Idaho National Laboratory and the National Science Foundation Graduate Research Fellowship Grant No. 1122374. This research made use of the resources of the High Performance Computing Center at Idaho National Laboratory, which is supported by the Office of Nuclear Energy of the U.S. Department of Energy and the Nuclear Science User Facilities under Contract No. DE-AC07-05ID14517.

References

Boyd, W., Forget, B., Smith, K., 2015. OpenCG: A Combinatorial Geometry Modeling Tool for Data Processing and Code Verification. In: Int'l Conf. on Mathematics and Computational Methods Applied to Nuclear Science & Engineering. Nashville, TN, USA.

Boyd, W., Romano, P. K., Harper, S., 2016a. Equipping OpenMC for the Big Data Era. In: PHYSOR. Sun Valley, ID, USA.

Boyd, W., Shaner, S., Li, L., Forget, B., Smith, K., 2014. The OpenMOC Method of Characteristics Neutral Particle Transport Code. Annals of Nuclear Energy 68, 43–52.

Boyd, W., Siegel, A., He, S., Forget, B., Smith, K., 2016b. Parallel Performance Results for the OpenMOC Neutron Transport Code on Multicore Platforms. Int'l Journ. of High Performance Computing Applications.

Boyd, W. R. D., 2016. Reactor Agnostic Multi-Group Cross Section Generation for Fine-Mesh Deterministic Neutron Transport Simulations. Ph.D. thesis, Massachusetts Institute of Technology (submitted).

Cai, L., 2014. Condensation and Homogenization of Cross Sections for the Deterministic Transport Codes with Monte Carlo Method: Application to the GEN IV Fast Neutron Reactors. Ph.D. thesis, Université Paris Sud-Paris XI.

Horelik, N., Herman, B., Forget, B., Smith, K., 2013. Benchmark for Evaluation and Validation of Reactor Simulations (BEAVRS), v1.0.1. In: Int. Conf. Math. and Comp. Methods Applied to Nuc. Sci. & Eng. Sun Valley, Idaho, USA.

Lax, D., Boyd, W., Horelik, N., 2014. An Algorithm for Identifying Unique Regions in Constructive Solid Geometries. In: PHYSOR. Kyoto, Japan.

Leppänen, J., 2013. Serpent – A Continuous-Energy Monte Carlo Reactor Physics Burnup Calculation Code. VTT Technical Research Centre of Finland.

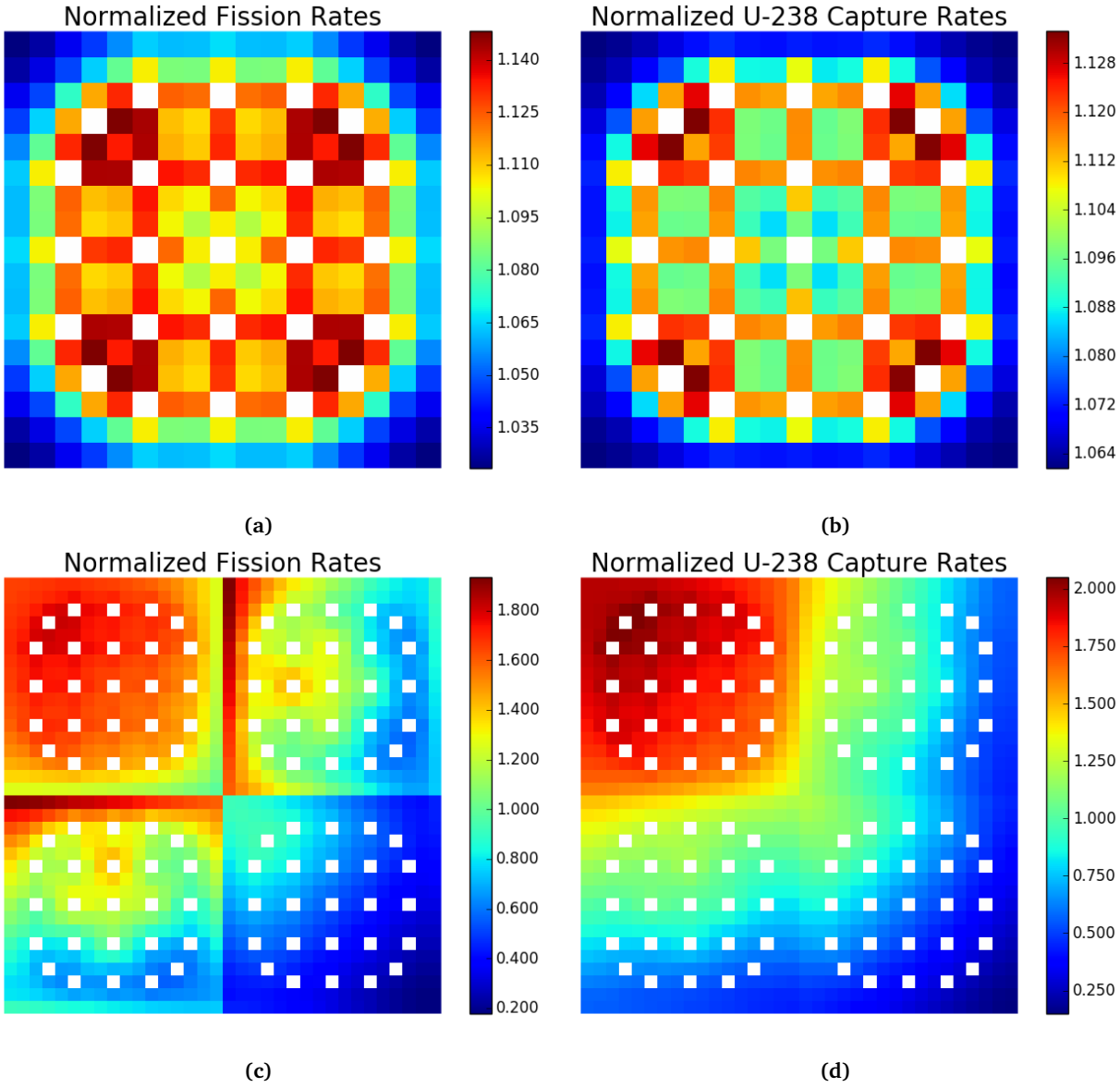

Figure 4. Fission and U-238 capture rates for the (a) – (b) assembly and (c) – (d) colorset.

National Nuclear Data Center, Brookhaven National Laboratory, 2016. ENDF/B-VII.1 Evaluated Nuclear Data Library. http://www.nndc.bnl.gov/endf/b7.1/, accessed: 2016-08-09.

Nelson, A., 2014. Improved Convergence Rate of Multi-Group Scattering Moment Tallies for Monte Carlo Neutron Transport Codes. Ph.D. thesis, University of Michigan.

Redmond, E. L., 1997. Multi-Group Cross Section Generation via Monte Carlo Methods. Ph.D. thesis, Massachusetts Institute of Technology.

Rhodes, J., Smith, K., Lee, D., 2006. Casmo-5 development and applications. In: ANS Topical Meeting on Reactor Physics (PHYSOR). pp. 10–14.

Romano, P. K., Forget, B., 2013. The OpenMC Monte Carlo Particle Transport Code. Annals of Nuclear Energy 51, 274–281.

X-5 Monte Carlo Team, 2003. MCNP-A General Monte Carlo N-Particle Transport Code, Version 5. , Los Alamos National Laboratory.

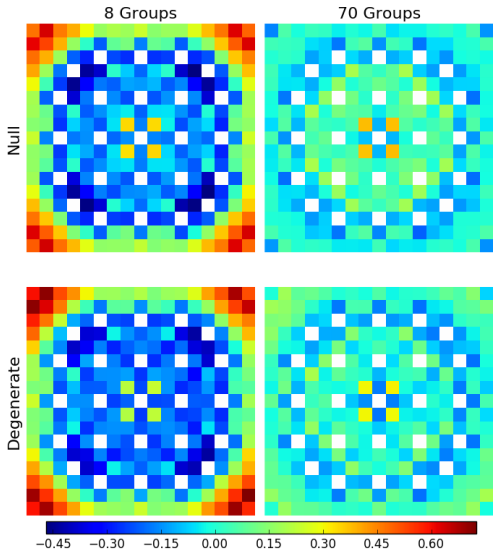

(a)

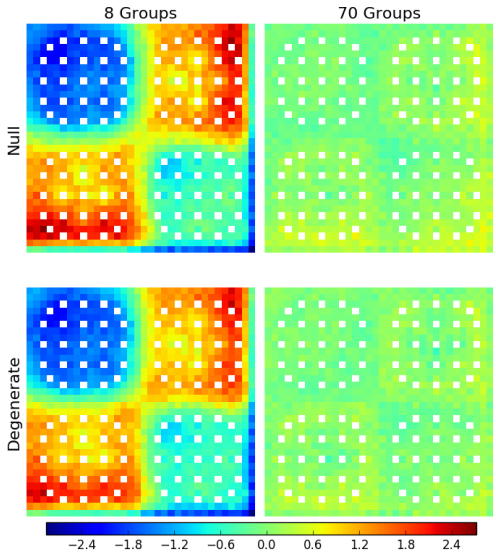

(b)

Figure 5. OpenMOC fission rate percent relative errors for the (a) assembly and (b) 2×2 colorset models.

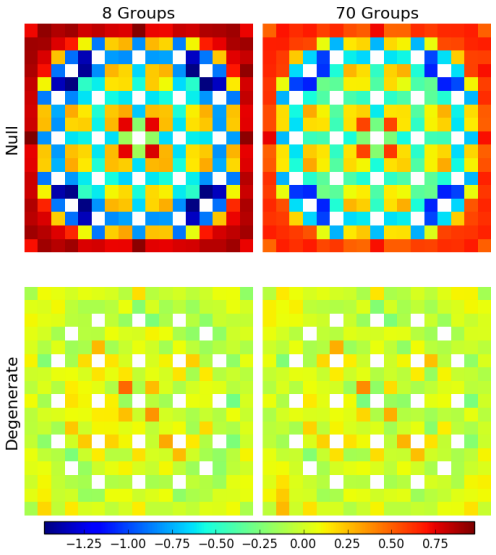

(a)

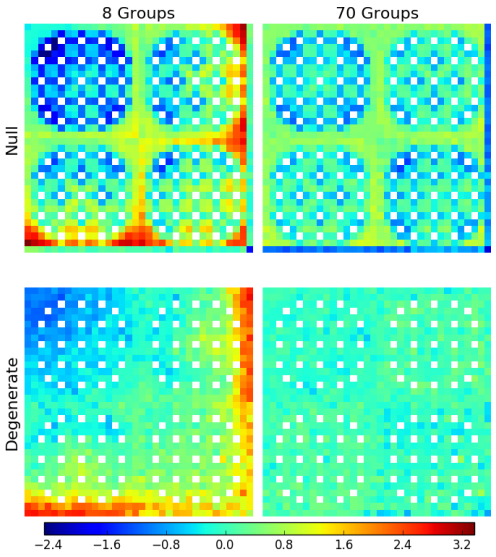

(b)

Figure 6. OpenMOC U-238 capture rate percent relative errors for the (a) assembly and (b) 2×2 colorset models.